actuators

MDPI

Article

Design and Unbiased Control of Nine-Pole Radial Magnetic Bearing

Myounggyu D. Noh * and Wonjin Jeong

Department of Mechatronics Engineering, Chungnam National University, Daejeon 34134, Republic of Korea
* Correspondence: mnoh@cnu.ac.kr; Tel.: +82-42-821-6877

Abstract: Typical radial active magnetic bearings are structurally symmetric. For example, an eight-pole bearing uses two opposing pairs to control one axis by winding the pair in series. The magnetic force produced by an active magnetic bearing is quadratically proportional to coil currents and inversely proportional to the square of the gap between the bearing and the journal. Bias linearization is widely used to linearize the relationship of coil currents to the magnetic force. However, the bias currents increase ohmic losses and require a larger than necessary capacity of power amplifiers to supply the sum of bias and control currents. Unbiased control of symmetric bearings has the critical issue of slew-rate limiting. Unbiased control of unsymmetrical bearings can eliminate the need for bias currents while avoiding slew-rate singularity except in extreme cases. Although a generalized inversion of the force–current relationship of unbiased unsymmetrical bearings has been proposed previously, no experimental validation is reported. The main objective of this research is to implement the unbiased control strategy and show that exactly the same linear control strategy for eight-pole symmetric bearings can be applied to nine-pole unsymmetrical bearings on industry-scale compressor test rigs. Two test rigs are built: one with eight-pole symmetric bearings and another with nine-pole unsymmetrical bearings. Linear control algorithms are designed and applied. Both control algorithms are linear and consist of lead filters and notch filters. The test results show that the linear control design used for unsymmetrical bearings can achieve the same level of stability that the symmetric bearings provide, satisfying the sensitivity criterion specified by ISO 14839-3.

Keywords: active magnetic bearings (AMBs); unsymmetric bearing; unbiased control

Citation: Noh, M.D.; Jeong, W. Design and Unbiased Control of Nine-Pole Radial Magnetic Bearing. *Actuators* **2023**, *12*, 458. https://doi.org/10.3390/act12120458

Academic Editor: Takeshi Mizuno

Received: 20 October 2023
Revised: 24 November 2023
Accepted: 7 December 2023
Published: 9 December 2023

1. Introduction

Active magnetic bearings (AMBs) use magnetic forces to levitate the rotor without mechanical contact, thereby enhancing system efficiency, increasing operating speed and improving the reliability of the machine [1]. They are open-loop unstable, and require feedback control using the position of the rotor to maintain the levitation.

The magnetic forces generated from coil currents of AMBs are quadratic to the coil currents and inversely quadratic to the gap between the stator and the target. When symmetric radial bearings are used, bias linearization is typically used to linearize the force–current relationship so that linear control algorithms can be used. For example, an eight-pole bearing uses two opposing pairs to control one axis by winding the pair in series. The coil currents to the opposing pairs are either the sum or differential of the constant bias current and control current [2,3]. However, bias currents increase ohmic losses and require a larger than necessary capacity of the power amplifier for supplying coil currents.

In the literature, many attempts to either remove or reduce bias currents can be found. Power-minimizing control algorithms that eliminate bias currents [4–6] involve some form of switching. For example, Sivrioglu et al. [5] used a switching scheme to obtain a feedback-linearized plant model and then designed a H_∞ control. Mystkowski and Pawluszewicz [6] also used a voltage-switching scheme, but reduced the complexity of the control by using control Liapunov functions. However, these zero-bias control algorithms are affected

by the singularity of the force slew rate if the force command becomes zero. Low-bias algorithms [7–10] adjust bias currents according to adaptive or predetermined rules, but may be subject to voltage saturation at a high force slew rate.

Several proposals of using structurally unsymmetrical bearings have been published in such a way as to eliminate bias currents. For example, bearings with three poles [11–13] can generate the forces in two orthogonal directions, although the forces are coupled. Even though the force coupling makes the inversion difficult, a finite force slew rate can be maintained except in the extreme cases where both force commands in two orthogonal axes are zero at the same time. The main drawback of three-pole bearings is that the bearing is adequate only for very small rotors, because the shaft carrying the rotor laminations becomes increasingly small as the bearing size gets large.

Other unsymmetrical configurations are possible for large bearings, such as six-pole bearings [14]. Meeker [15] proposed a general unbiased control strategy for various configurations of unsymmetrical bearings, and suggested an example of nine-pole bearings. However, none of the previous efforts provide the implementation of unbiased control and validate the control algorithms on an industry-scale test rig. In this paper, we demonstrate how the unbiased control algorithm can be implemented for a chiller compressor. A phase-selection algorithm is introduced to alleviate the effect of noise in the force inversion. For a fair evaluation of the unbiased control, another test rig with the symmetric bearings of the same capacity is built. With these two test setups, it is possible to show how linear control can be directly used for unbiased control if the gains are adjusted properly.

The content of the paper is as follows. Section 2 describes the force–current relationship of unsymmetrical bearings in comparison with common symmetrical eight-pole bearings. In Section 3, a design of a nine-pole unsymmetrical bearing is derived and compared with other design alternatives. Section 4 contains how the control algorithm is constructed for unsymmetrical bearings. Section 5 describes the two test rigs: one with symmetric bearings and the other with unsymmetrical bearings. Section 6 shows the results and discusses the main points of the paper. The last section concludes and summarizes the paper.

2. Force–Current Relationship

2.1. Radial Magnetic Bearing

Radial magnetic bearings support a rotor in radial directions using electromagnetic forces. Figure 1 shows one type of radial magnetic bearing. There are a total of eight poles, each of which carries a coil winding. Two adjacent poles are wired in series, so that magnetic polarities of the poles alternate when a current is injected. This type of bearing is commonly called a heteropolar horseshoe configuration [1]. Opposing pairs of horseshoes produce bi-directional force in one degree of freedom. Thus, a total of four currents are required to levitate the rotor.

The geometry of a radial bearing is defined by several variables. The outermost size of the bearing stator is the stator radius, r_s. The width of the stator back iron is determined by the difference between r_s and the inner radius r_c. The radial pole length ($r_c - r_p$) is largely determined by the required coil turns. The journal radius, r_j, determines the rotor size at the bearing location. In most cases, a stack of laminated sheets of electrical steel such as silicon iron is used for the flux path. The stator is entirely made of laminations, while the rotor carries a lamination ring on a shaft, which is necessary for structural rigidity and assembly. To maintain a uniform magnetic path size, a typical bearing design assumes that

$$w = r_j - r_r \ . \tag{1}$$

The nominal air gap is defined as

$$g_0 = r_p - r_j \ . \tag{2}$$

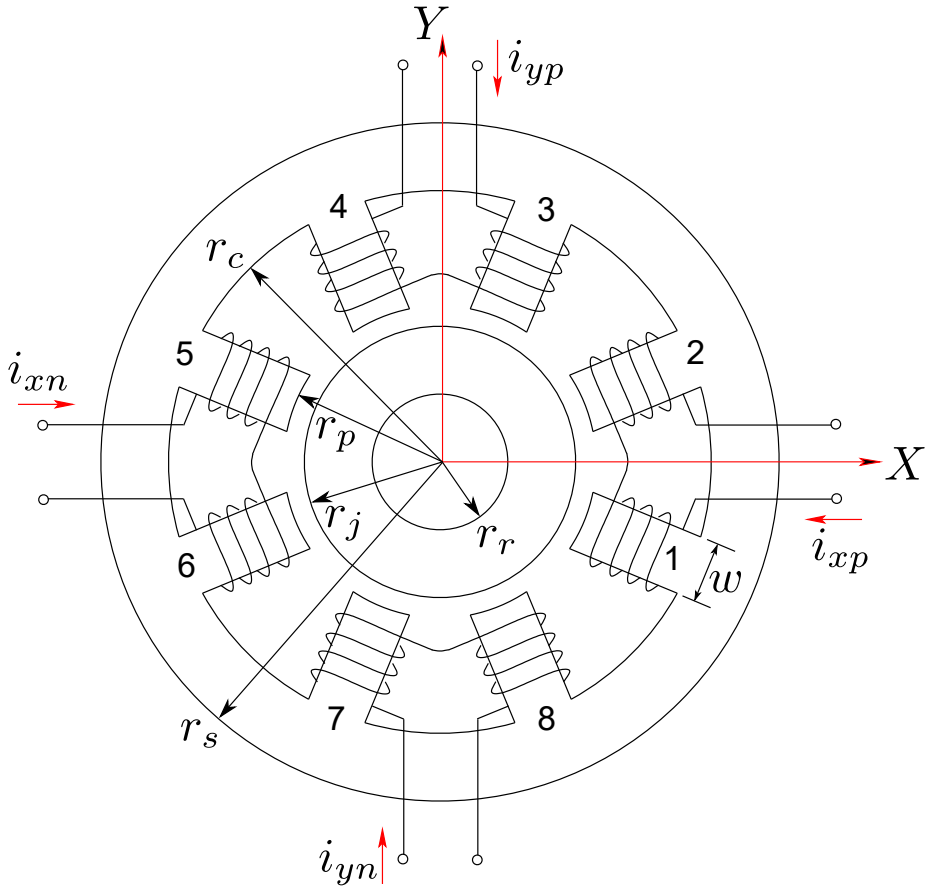

Figure 1. Structure of a heteropolar radial magnetic bearing. For illustrative purposes, the horseshoe configuration of an eight-pole bearing is shown.

2.2. Force vs. Coil Currents

Coil currents produce magnetic fields in the bearing, which in turn generate attractive forces on the rotor. The relationship between coil currents and the resulting forces can be obtained using magnetic circuit theory [16,17]. Assuming that the stator and rotor laminations are made of highly permeable material, the reluctances of the stator and rotor can be neglected. The magnetic field densities at each air gaps, $\mathbf{b}$ can be expressed as

$$\boldsymbol{\mathcal{R}}\mathbf{b} = \mathbf{N}\mathbf{i}\,, \tag{3}$$

where $\boldsymbol{\mathcal{R}}$ and $\mathbf{N}$ are the reluctance and coil turn matrices, respectively. For the eight-pole symmetric bearing shown in Figure 1, these matrices are given in (A1) and (A2) in Appendix A. The coil current vector is

$$\mathbf{i} = [i_{xp}\ i_{yp}\ i_{xn}\ i_{yn}]^T\,.$$

The attractive forces can then be written as

$$f_x = \mathbf{b}^T\mathbf{A}_x\mathbf{b}\,, \tag{4}$$

$$f_y = \mathbf{b}^T\mathbf{A}_y\mathbf{b}\,, \tag{5}$$

where pole area matrices are defined as

$$\mathbf{A}_x = \frac{A_p}{2\mu_0}\text{diag}(\cos\theta_i)\ , \tag{6}$$

$$\mathbf{A}_y = \frac{A_p}{2\mu_0}\text{diag}(\sin\theta_i)\ . \tag{7}$$

Here, A_p is the cross-sectional area of poles and θ_i is the angle of the i-th pole. Combining (3) with (6) and (7), we obtain

$$f_m = \mathbf{i}^T\mathbf{M}_m\mathbf{i},\ \ m = x, y\ , \tag{8}$$

where $\mathbf{M}_m = \mathbf{N}^T\boldsymbol{\mathcal{R}}^{-T}\mathbf{A}_m\boldsymbol{\mathcal{R}}\mathbf{N}$. Equation (8) can be written in the form of scalar equations. For example, the force in the x-direction is

$$f_x = \frac{\mu_0 A_p N^2\cos\theta_p}{4}\left[\frac{i_{xp}^2}{(g_0 - x\cos\theta_p)^2} - \frac{i_{xn}^2}{(g_0 + x\cos\theta_p)^2}\right]\ , \tag{9}$$

where θ_p is half of the angle between two adjacent poles.

The force–current relation of (8) is quadratic and not unique. To make this unique, a bias current is introduced.

$$\begin{bmatrix} i_{xp} \\ i_{yp} \\ i_{xn} \\ i_{yn} \end{bmatrix} = \begin{bmatrix} 1 & 0 & 1 \\ 0 & 1 & 1 \\ -1 & 0 & 1 \\ 0 & -1 & 1 \end{bmatrix}\begin{bmatrix} i_x \\ i_y \\ I_b \end{bmatrix} = \mathbf{W}\mathbf{i}_c, \tag{10}$$

where I_b is the fixed bias current. Assuming that the control currents, i_x and i_y, are smaller than the bias current, Equation (8) can be linearized [2,3].

$$f_m = -K_s m + K_i i_m,\ \ m = x, y\ , \tag{11}$$

where K_i is the actuator gain and K_s is the open-loop stiffness, which is negative in sign.

2.3. Unsymmetrical Bearing

As stated above, a bias current is used to linearize the force–current relationship of a symmetric eight-pole bearing. Due to the bias current, ohmic losses in the stator coils as well as the capacity of the amplifier increase. Many attempts to reduce (or remove) the bias current have been made (e.g., [8,9]) without much success due to the singularity in the force slew rate at zero bias or excessive voltage requirement at low bias.

A different approach to eliminating the bias current is to use unsymmetrical bearings. The most common unsymmetrical bearing is the bearing with three poles [11,13]. As stated in the introduction, three-pole bearings are only applicable for very small rotors. If the pole width becomes large to accommodate the required load capacity of a three-pole bearing, the rotor radius, r_r, becomes small as shown in (1). A small shaft lowers the bending mode frequencies, decreasing the separation margin [18].

Variations in the three-pole structure for large bearings include six-pole [14] and nine-pole bearings [15]. Figure 2 illustrates the winding pattern of the nine-pole bearing. Three adjacent poles are wired in series, forming one phase. The winding direction is specified with either $+$ or $-$: $+$ means the flux flowing into the journal and $-$ means the flux flowing in the opposite direction. The force–current relationship of this nine-pole bearing can be expressed by (8) if the reluctance and coil turn matrices are defined accordingly. The

reluctance matrix can be constructed very similarly to (A1). The coil turn matrix is defined in (A3). Then, the bearing force is obtained from

$$f_m = \begin{bmatrix} i_A & i_B & i_C \end{bmatrix} \mathbf{M}_m \begin{bmatrix} i_A \\ i_B \\ i_C \end{bmatrix}, \quad m = x, y \,. \tag{12}$$

The force–current relation (12) is not one-to-one, and thus not invertible. Control currents corresponding to control commands can be introduced such that

$$\begin{bmatrix} i_A \\ i_B \\ i_C \end{bmatrix} = \mathbf{W} \begin{bmatrix} i_r \\ i_i \end{bmatrix} \tag{13}$$

If the mapping matrix satisfies

$$\mathbf{W}^T \mathbf{M}_x \mathbf{W} = \begin{bmatrix} 1 & 0 \\ 0 & -1 \end{bmatrix} \tag{14}$$

$$\mathbf{W}^T \mathbf{M}_y \mathbf{W} = \begin{bmatrix} 0 & 1 \\ 1 & 0 \end{bmatrix}, \tag{15}$$

we can express the force–current relationship in complex form [13,15]:

$$f_x + j f_y = c(i_r + j i_i)^2 \,, \tag{16}$$

where the constant is defined as

$$c = \frac{\mu_0 N^2 A_p}{g_0} \,.$$

The mapping matrix in (14) and (15) is not unique. Ref. [15] proposes an optimization process where both the average flux level in the stator and the coil currents (thus ohmic losses) are minimized. Through this optimization process, the mapping matrix for the nine-pole bearing of Figure 2 is found to be [15]

$$\mathbf{W} = \begin{bmatrix} 1.026 & 0 \\ -0.5131 & -0.8887 \\ -0.5131 & 0.8887 \end{bmatrix} \tag{17}$$

for the case where the x-axis is aligned with the A-phase coil as shown in Figure 2. Note that the column sums of the mapping matrix (17) are zero, which means that the phase currents are balanced.

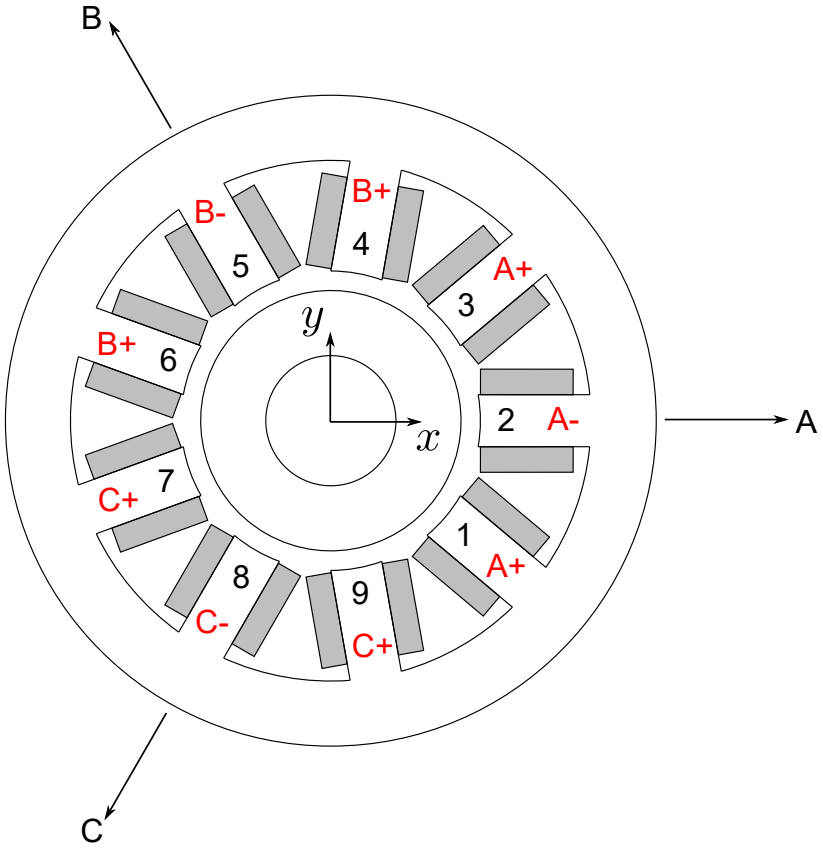

Figure 2. Structure of an unsymmetrical radial bearing with nine poles. Three adjacent poles are wired in series. A single three-phase drive can be used to power the bearing.

3. Unsymmetrical Bearing Design

3.1. Reference Symmetric Bearing

To conduct an objective comparison of unsymmetrical bearing designs, we select a reference design of an eight-pole symmetric bearing. The bearing is used in a turbo-chiller compressor. The load capacity is 1120 N. Table 1 lists the design parameters of the bearing.

Table 1. Design parameters of the eight-pole reference bearing.

Parameter	Symbol	Value	Unit
Nominal gap	g_0	0.5	mm
Number of coil turns	N	32	
Journal radius	r_j	46.6	mm
Pole width	w	16.6	mm
Rotor shaft radius	r_r	30	mm
Stator outer radius	r_s	77	mm
Stator mass	m_{stator}	4.5	kg
Actuator gain	K_i	141	N/A
Open-loop stiffness	K_s	−1826	N/mm

3.2. Comparison of Unsymmetrical Designs

Several unsymmetrical design alternatives with a different number of poles are considered. The axial length of the bearing is fixed, as are the air gap and the journal diameter. The size of the bearing is determined so that any parts of the bearing (journal ring, pole

sections and stator back irons) do not reach saturation while producing the required load capacity. The pole face area of the bearing, A_p, is related to the load capacity as

$$F_{\text{load}} = f_{\text{load}} \frac{B_{\text{sat}}^2 A_p}{\mu_0} \tag{18}$$

where the load factor, f_{load}, is determined when obtaining the mapping matrix for unsymmetrical bearings, since the optimization takes the flux density levels into account [15]. If the axial length of the bearing is fixed, the pole width can be simply the pole face area divided by the axial length. The stator back iron size is also determined from the optimization process [15]. The minimum stator path thickness is the size below which the saturation occurs in the stator. The ratio of the stator path thickness to the pole width is defined as

$$\alpha = \frac{r_s - r_c}{w} \tag{19}$$

Table 2 lists the design cases. The six-pole case has a horseshoe configuration; therefore, α is equal to one. The nine-pole case has a winding configuration as shown in Figure 2.

The design results are also summarized in Table 2. Stator size, stator mass and rotor size are all ratios with respect to the reference design of Table 1. The thee-pole case has the largest stator size, which is 38% larger and about three times heavier than the reference design. It is possible to decrease the stator size if full-fill winding is used instead of the straight-fill method, although the winding would be much more difficult. More problematic is the rotor size, which is only 19% of the reference design. The more slender the shaft becomes, the lower the flexible mode frequencies. Since the mass of the journal increases, the lowering of the mode frequencies would be more significant when the rotor diameter shrinks.

The five-pole design results in a slightly smaller stator, which is advantageous. However, the shaft size is still too small (72% of the reference design). Also, a five-phase drive is necessary, which is rather uncommon. Alternatively, two sets of the three-phase drive can supply currents to the bearing. The six-pole design is a variation of the three-pole bearing with horseshoe winding. The rotor shaft is still smaller than the reference design, but the stator size is almost the same.

The nine-pole design shows that the stator is smaller than the reference design, while the rotor size is essentially the same. Since three adjacent poles are wired in series, a single three-phase drive can be used as a power amplifier for the bearing. This is a significant advantage over the eight-pole symmetric bearing. If biased control is used, at least eight power switches are necessary to drive a radial bearing even if a half-bridge configuration is adopted. Since many commercial power modules come in three-phase six-switch packages, there may be cases when some of the switches are not utilized if these commercial power modules are used to drive the biased eight-pole bearing. Lowering the power switch count not only save costs but also improve the reliability of the power amplifier.

Table 2. Several design cases of unsymmetrical bearing (all entries are non-dimensional, and the sizes are ratios to the reference design).

Pole Count	f_{load} (18)	α (19)	Stator Size	Stator Mass	Rotor Size
3	0.375	0.578	1.38	2.96	0.19
5	0.625	0.526	0.90	0.78	0.72
6	0.650	1.000	1.03	1.26	0.75
9	0.950	0.670	0.94	0.74	1.01

4. Unbiased Control Design

4.1. Force Inversion

To construct a control for levitation, we need the inversion of the force–current relationship (16)

$$i_r^* = \frac{1}{\sqrt{2}}\sqrt{\sqrt{f_x^2 + f_y^2} + f_x}\,, \tag{20}$$

$$i_i^* = \frac{\mathrm{sgn}(f_y)}{\sqrt{2}}\sqrt{\sqrt{f_x^2 + f_y^2} - f_x}\,, \tag{21}$$

where $\mathrm{sgn}(\cdot)$ takes either a plus or minus sign depending on the sign of the argument. When inverting the force equation, it is important to maintain the phase so that large changes in current commands can be prevented. This issue has been discussed in [12] for a three-pole bearing. Here, the phase selection is described from a slightly different perspective.

Assume that the force command is close to the negative real axis in the complex plane. In other words, the force command can be expressed as

$$F_1 = F_0\, e^{j(\pi-\delta)}\,,$$

where the angle δ is positive and close to zero (refer to Figure 3a). If the force command moves to the third quadrant, it can be written as

$$F_2 = F_0\, e^{j(-\pi+\delta)}$$

so that the phase angle lies between $-\pi$ and π. Then, the current commands are

$$I_1 = I_0\, e^{j(\pi-\delta)/2} \approx jI_0\,,$$

$$I_2 = I_0\, e^{j(-\pi+\delta)/2} \approx -jI_0\,.$$

Therefore, a large jump in current command can be produced if the force command crosses the negative real axis. This can be remedied by adding 2π when there is a jump. Then,

$$\Delta I = |I_2 - I_1| = 2I_0 \sin\frac{\delta}{2}$$

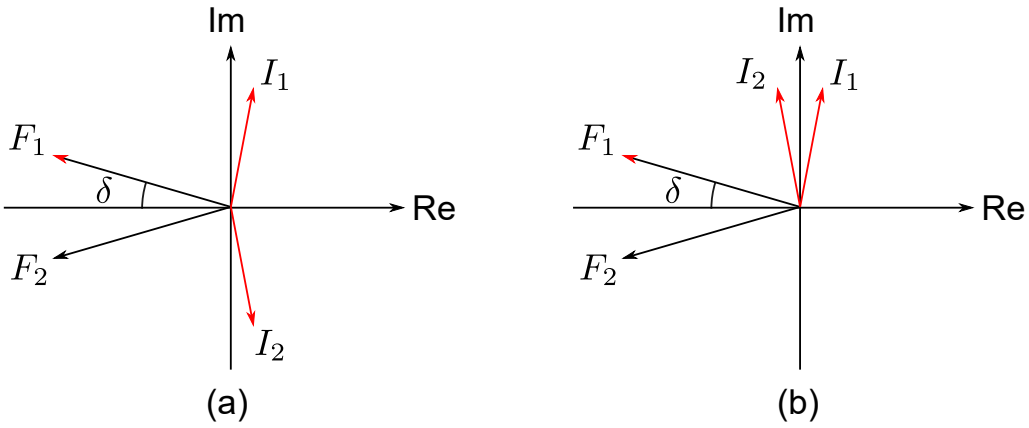

Figure 3. (**a**) If the force command is in the negative real axis, there can be a large jump in the current command. (**b**) Since the phase is 2π periodic, the large jump can be prevented by adding 2π to the phase.

4.2. Displacement Compensation

The magnetic force is not only dependent on the coil currents but also affected by the air gap between the pole tip and the journal of the bearing. For typical radial bearings, the force is inversely proportional to the square of the air gaps, as shown in (9). If the displacement of the rotor is small as compared to the air gap, the force equation can be linearized with respect to the displacements. For unsymmetrical bearings, this linearization is equivalent to the modification of current command such that [15]

$$i_r = i_r^* - (x/g_0)i_r^* - (y/g_0)i_i^* \,, \tag{22}$$

$$i_i = i_i^* - (y/g_0)i_r^* + (x/g_0)i_i^* \,, \tag{23}$$

where i_r^* and i_i^* are the current commands obtained from the force inversion (20). Figure 4 shows the block diagram of the unbiased control for active magnetic bearings. The blocks enclosed by dotted lines contain nonlinearities of the system: force inversion rule and displacement compensation. Once these nonlinearites are included in the plant, the input–output relationship of the plant becomes linear because the forces generated by the bearing, f_x and f_y, are linear to the control commands f_x^* and f_y^*. Therefore, it is possible to use linear control algorithms such as lead–lag compensators.

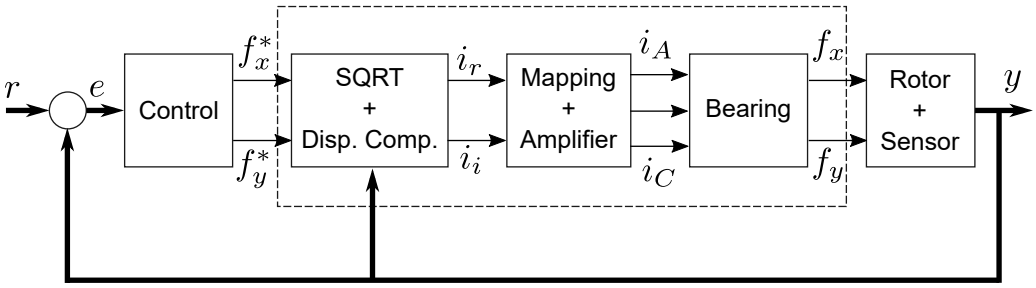

Figure 4. Block diagram of the unbiased control. The signals r, e and y are vectors containing both x and y components.

4.3. Unbiased Control Design

Active magnetic bearings are open-loop unstable. The most common control algorithm to stabilize the bearing is a proportional-derivative (PD) type. It is also called a lead filter because the derivative action provides a positive phase. In this paper, we use a PID-type controller that consists of a lead filter with complex poles [19] and an integrator, as shown in (24).

$$C_{\text{PID}} = K_P \frac{\tau_z^2 s^2 + 2\zeta_z \tau_z s + 1}{\tau_p^2 s^2 + 2\zeta_p \tau_p s + 1} + \frac{K_I}{s} \,. \tag{24}$$

The controller is added with notch filters to suppress the excitations of flexible modes of the rotor. Depending on the number of flexible modes in the control bandwidth, N_f, the notch filter can be expressed as

$$C_{\text{NF}} = \prod_{k=1}^{N_f} \frac{s^2 + 2\zeta_{nz,k}\omega_{nf,k}s + \omega_{nf,k}^2}{s^2 + 2\zeta_{np,k}\omega_{nf,k}s + \omega_{nf,k}^2} \,. \tag{25}$$

The controller may also need a low-pass filter to reduce the effects of sensor noise in the high frequencies. Thus, the bearing controller can be expressed as

$$C(s) = C_{\text{PID}} C_{\text{NF}} C_{\text{LPF}} \,. \tag{26}$$

When determining the proportional gain, K_P in (24), we need to consider the static gain of the error-to-force relationship. Referring to Figure 4 and (16), the static gain from error to force is

$$\left.\frac{f}{e}\right|_{s=0,\text{unbiased}} = \frac{\mu_0 N^2 A_p}{g_0^2} K_{P,\text{unbiased}} K_{\text{amp}} \,, \tag{27}$$

if the integrator is not considered. Here, K_{amp} is the dc gain of the amplifier. Figure 5 shows the block diagram of the bias-linearized bearing controller. Referring to (11), the corresponding static gain is

$$\left.\frac{f}{e}\right|_{s=0,\text{biased}} = K_{P,\text{biased}} K_{\text{amp}} K_i \,. \tag{28}$$

Since the actuator gain of the eight-pole symmetric bearing is

$$K_i = \frac{\mu_0 N^2 A_p I_b \cos\theta_p}{g_0^2}$$

the proportional gain of the unbiased control should be comparable to the counterpart of the bias-linearized control as

$$K_{P,\text{unbiased}} = K_{P,\text{biased}} I_b \cos\theta_p \tag{29}$$

if the nine-pole bearing is equivalently sized. Note that (29) does not indicate how the proportional gain of unbiased control is selected, but only shows the dc gain from error to force signals.

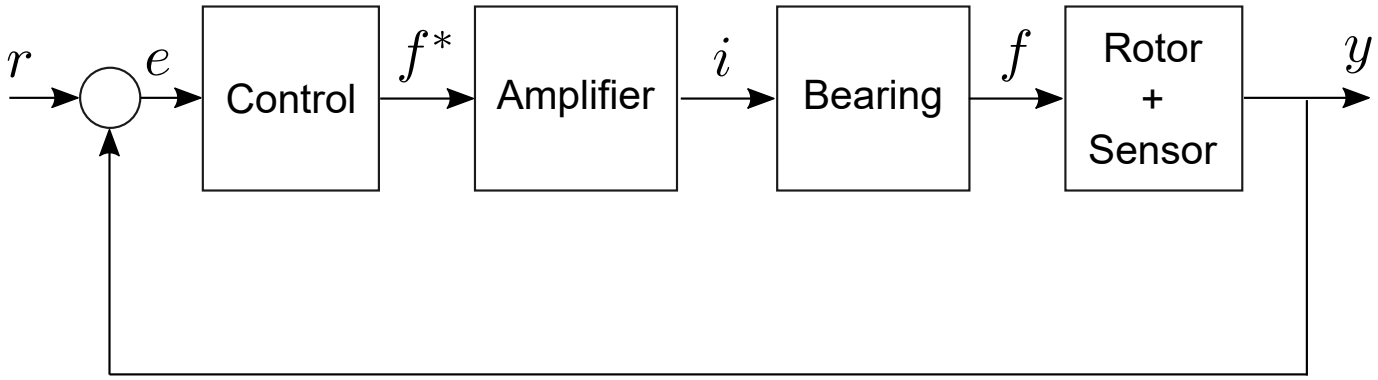

Figure 5. Block diagram of the linear control for active magnetic bearings. All signals are scalar quantities.

5. Experimental Setup

To implement and validate the logic of unbiased control, a test rig is set up. Nine-pole radial bearings with a load capacity of 1120 N and a size equivalent to the reference bearing of Table 1 are designed and constructed as shown in Figure 6a. The prototype compressor shown in Figure 6b is equipped with two nine-pole radial bearings and one thrust bearing.

The controller is implemented using MATLAB Simulink-RT at a sampling time of 0.1 ms. Three servo amplifiers (B060A400AC, Advanced Motion Controls) are used to generate the coil currents for each radial bearing. The prototype adopts position sensors that are internally developed using flexible printed-circuit technology.

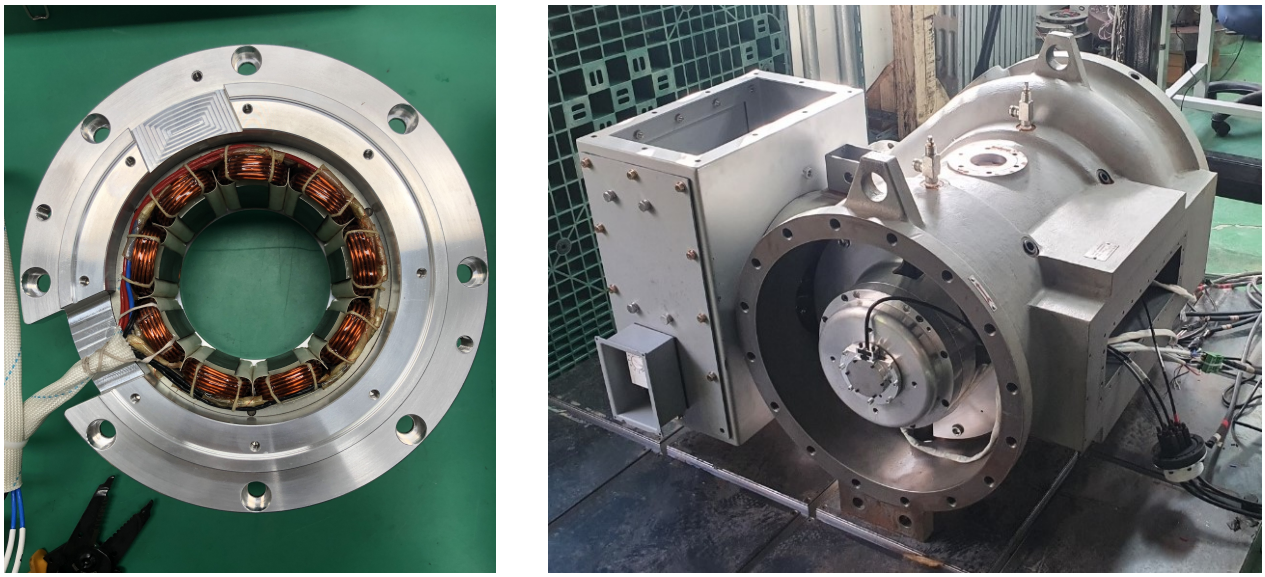

(**a**) 9-pole bearing (**b**) Prototype Compressor

Figure 6. Nine-pole unsymmetrical bearing and prototype compressor equipped with two nine-pole radial bearings.

For comparisons, another prototype compressor with eight-pole symmetric bearings (biased compressor) is built. The capacity of the compressor is the same as the one with nine-pole bearings (unbiased compressor). Thus, two compressors are identical in almost all aspects. The main difference is that the compressor with eight-pole bearings uses commercial position sensors (Bently Nevada 3300XL, Baker Hughes) while the unbiased compressor is equipped with in-house sensors. Due to the changes in the sensors, the rotor of the unbiased compressor is different from that of the biased compressor in terms of sensor locations and sensor target size. These differences result in the shifts in flexible mode frequencies.

6. Results and Discussion

Using sinesweep tests, it is possible to measure the plant transfer functions. Here, the plant includes everything that the controller sees. The unbiased plant seen by the controller is linear. Thus, the same sinesweep test procedure can be applied to both the biased and unbiased compressor. Figure 7 and Figure 8 show the measured plant transfer functions for the motor-side bearing and impeller-side bearing, respectively. Each bode plot contains the transfer functions in X and Y directions. As expected from a symmetric bearing, the transfer functions in X and Y directions are very similar. The first and the second bending mode frequencies are around 400 Hz and 770 Hz, respectively.

Figure 9 shows the plant transfer function of the motor-side bearing of the unbiased compressor, while Figure 10 displays the impeller-side plant transfer function. The bending frequencies are different from those of the biased compressor. It appears that the motor-side bearing has the first bending at 890 Hz and the second at 1100 Hz. For the impeller-side bearing, the bending frequencies are 490 Hz and 1400 Hz. As stated above, the disparities in bending frequencies are due to the differences in the sensor locations and the sensor target size.

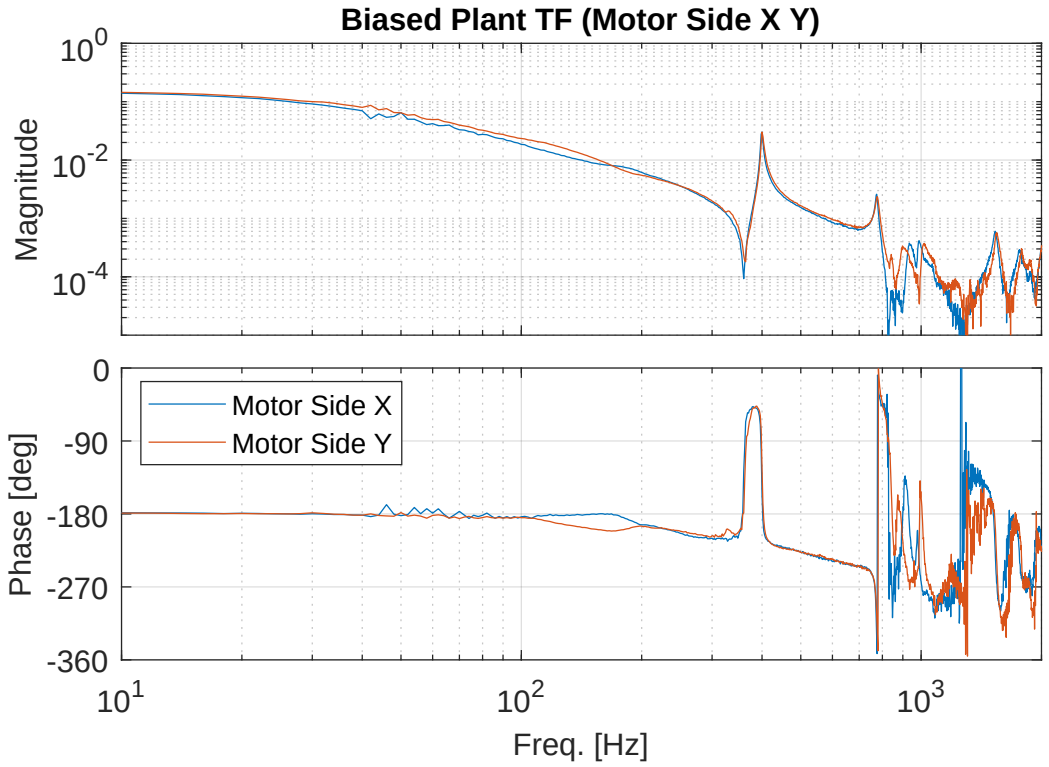

Figure 7. Biased compressor plant transfer functions (X and Y axis of motor-side bearing), which are measured through sinesweep tests.

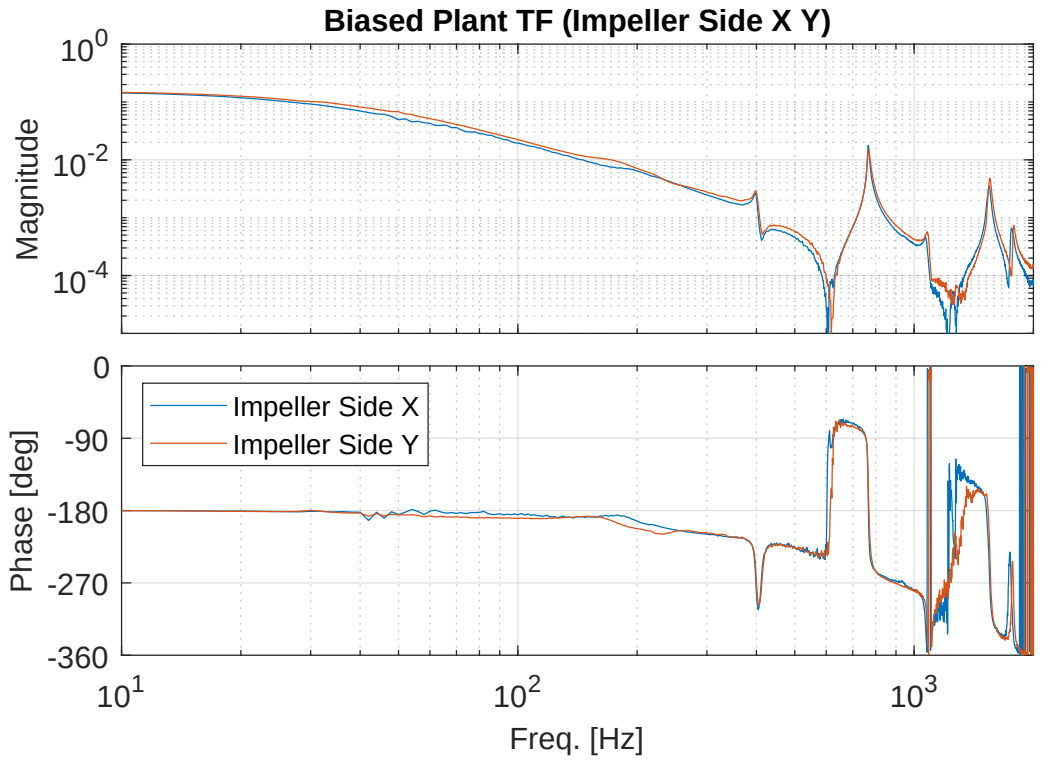

Figure 8. Biased compressor plant transfer functions (X and Y axis of impeller-side bearing).

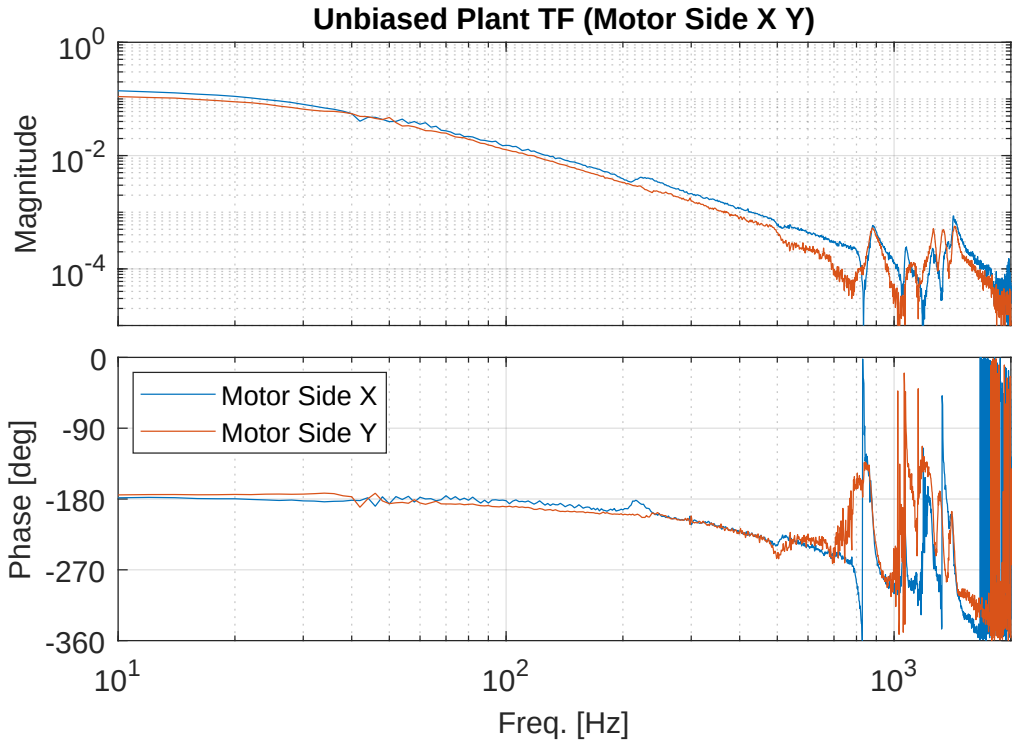

Figure 9. Unbiased compressor plant transfer functions (motor-side bearing X and Y).

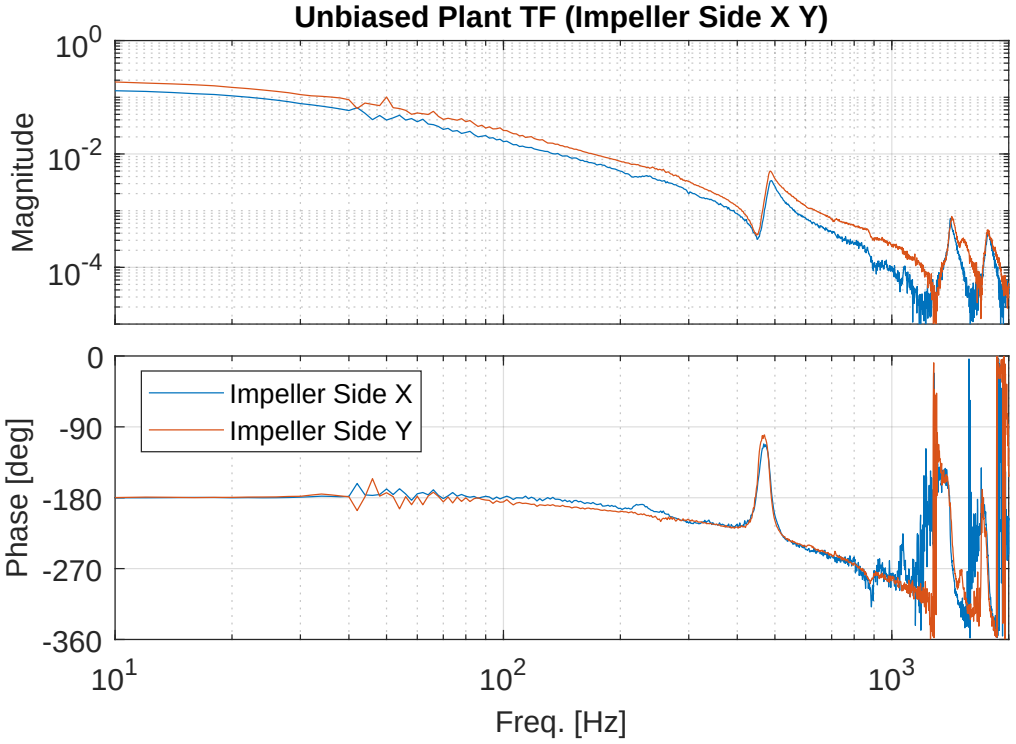

Figure 10. Unbiased compressor plant transfer functions (impeller-side bearing X and Y).

Another feature that is different in the plant transfer functions of two compressors is the gain at low frequencies. For symmetric bearings, it is expected that the plant transfer functions in X and Y directions are almost identical, since the force–current relationships should be the same in the two orthogonal directions. The nine-pole bearings used in the unbiased compressor are unsymmetrical, and thus the force–current relationship in X and

Y directions is different. Figure 11 shows the plant gains in low frequencies in absolute scale. For the biased compressor, the plant gains in X and Y directions are very close. The slight mismatch comes from the differences in the amplifier and sensor gains. The plant gains of the unbiased compressor shows that the mismatch is much larger than the biased case. Table 3 lists the plant gains at 10 Hz. The mismatch between X and Y directions of the biased compressor is 3.5% for the motor bearing and 12.3% for the impeller bearing. For the unbiased case, the mismatches are 21.0% for the motor bearing and 29.8% for the impeller bearing. If the same dynamical characteristics are required in X and Y directions, the gain disparity must be accounted for in the control design.

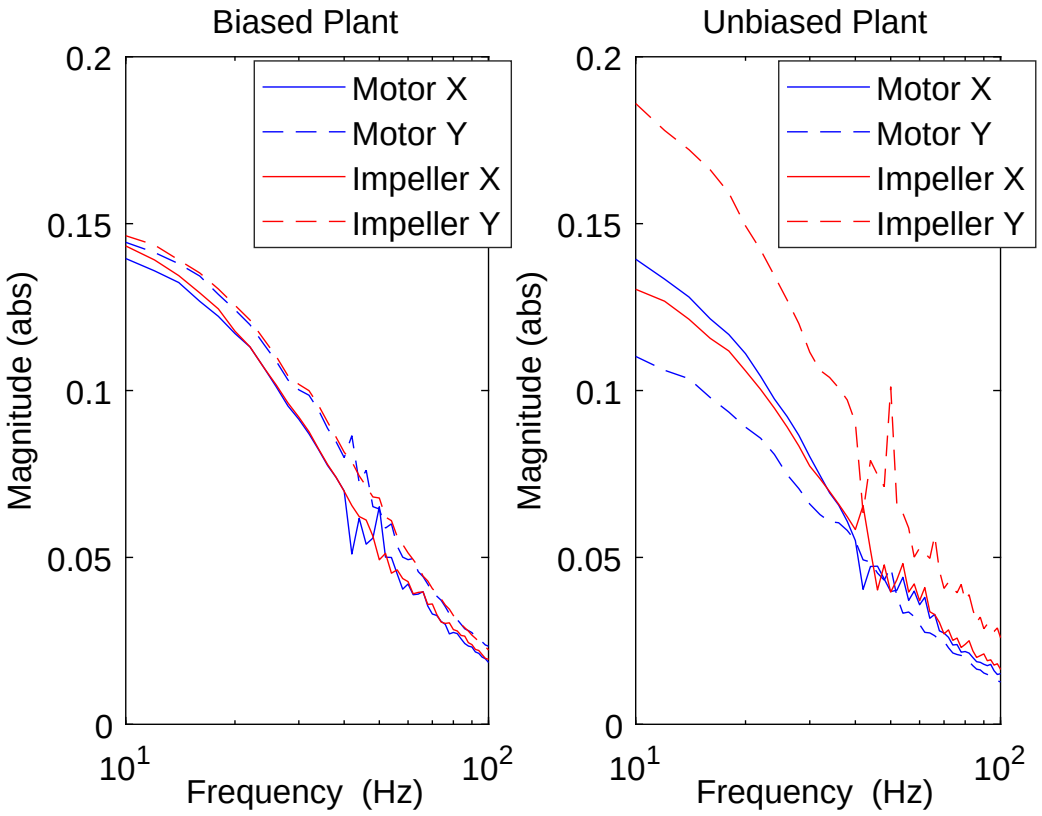

Figure 11. Gains of plant transfer functions in the frequency range from 10 to 100 Hz.

Table 3. Biased and unbiased compressor plant gain at 10 Hz.

Compressor	Bearing	X (mm/V)	Y (mm/V)	Ratio
Biased	Motor	0.1395	0.1444	1.035
	Impeller	0.1303	0.1464	1.123
Unbiased	Motor	0.1395	0.1102	0.790
	Impeller	0.1433	0.1860	1.298

Based on the plant transfer functions, controllers are designed for the biased and the unbiased bearings. Figure 12 and Figure 13 compare the bode plots of controllers for the motor-side and impeller-side bearings, respectively. When drawing the bode plots, the proportional gains of the unbiased control are adjusted according to (29) for the purpose of comparison. Since the flexible mode frequencies of the biased compressor are different from those of the unbiased machine, notch filters are applied at those corresponding frequencies.

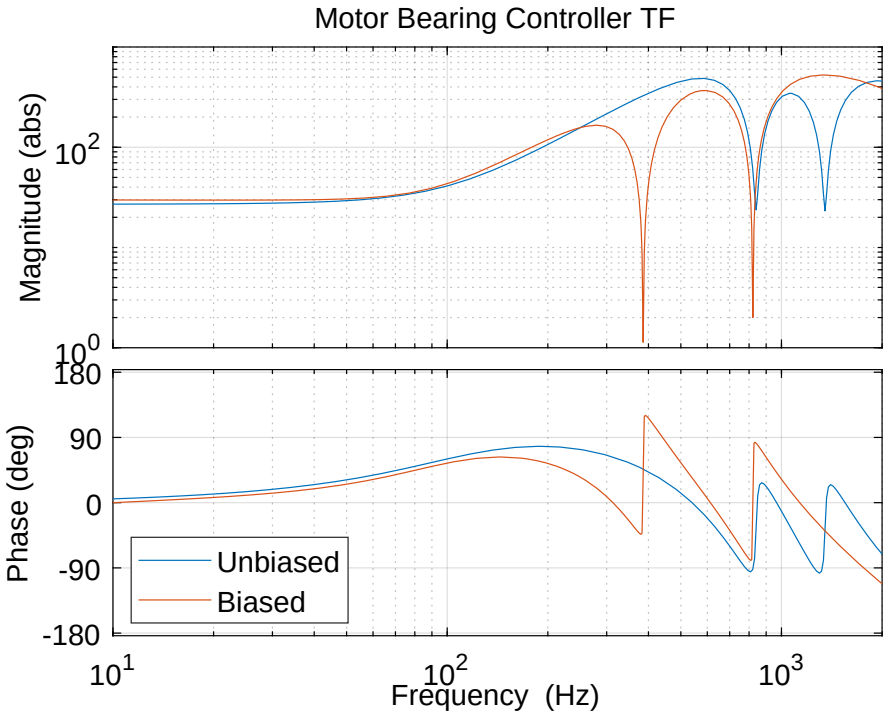

Figure 12. Bode plots of both biased and unbiased controller for motor bearing. Note that the proportional gain of unbiased control is adjusted according to (29) so that it can be compared with the biased control.

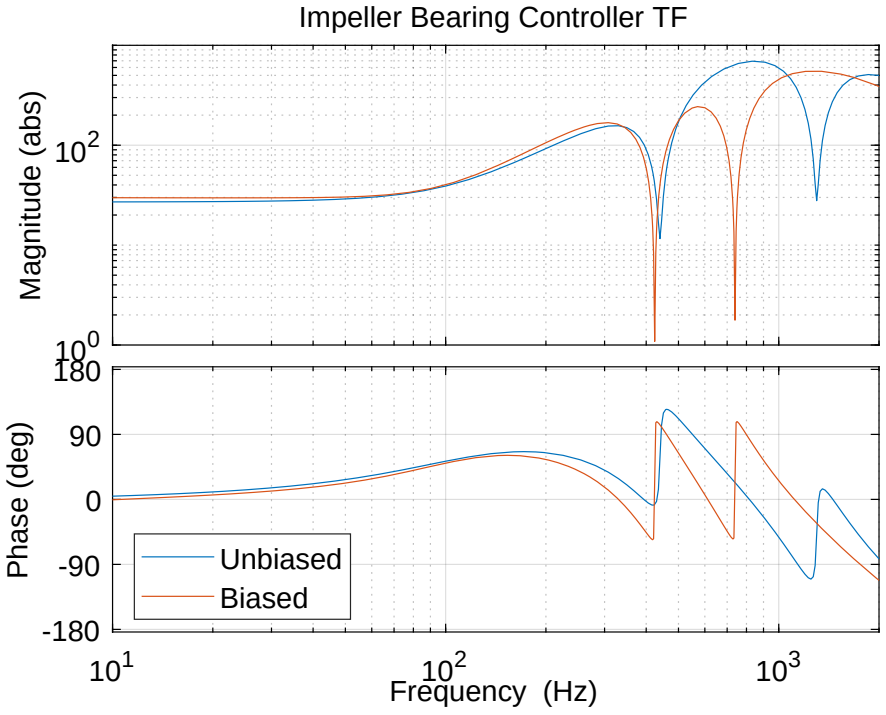

Figure 13. Bode plots of both biased and unbiased controller for impeller bearing.

Applying the controller of Figures 12 and 13, we obtain ample stability from the levitation control. Figures 14 and 15 show the output sensitivities of the unbiased control (motor-side and impeller-side bearing, respectively), which were measured from sinesweep tests. They are compared with those from the biased control for eight-pole bearings. According to ISO 14839-3 [20], the peak of the sensitivity must be below 3 (9.5 dB) for

continuous operation. Both biased and unbiased control maintain the sensitivity below 2, which indicates that the bearings can operate at the increased gains.

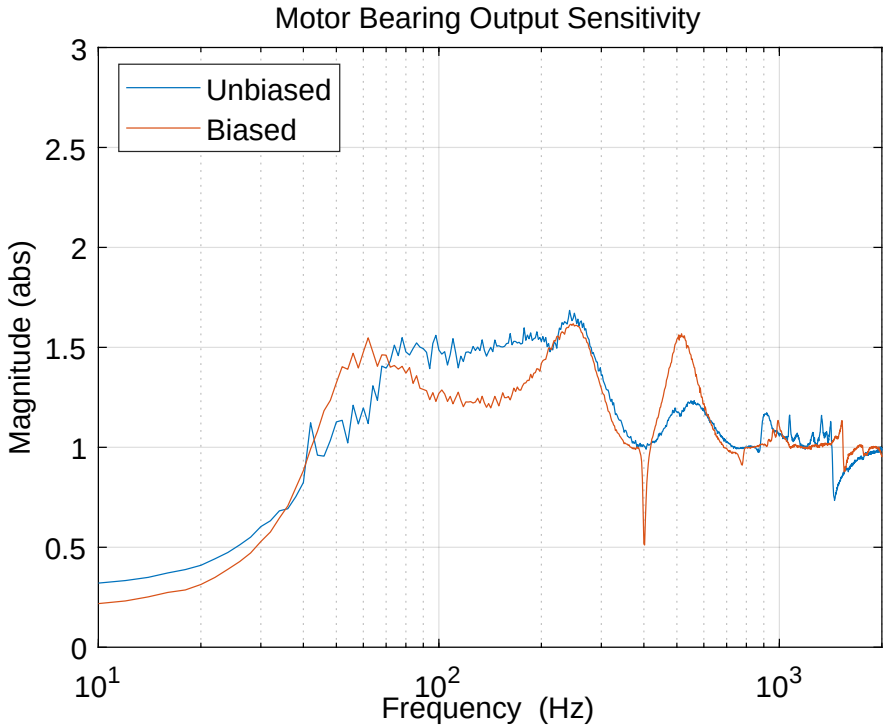

Figure 14. Comparison of output sensitivities of unbiased and biased control (motor bearing).

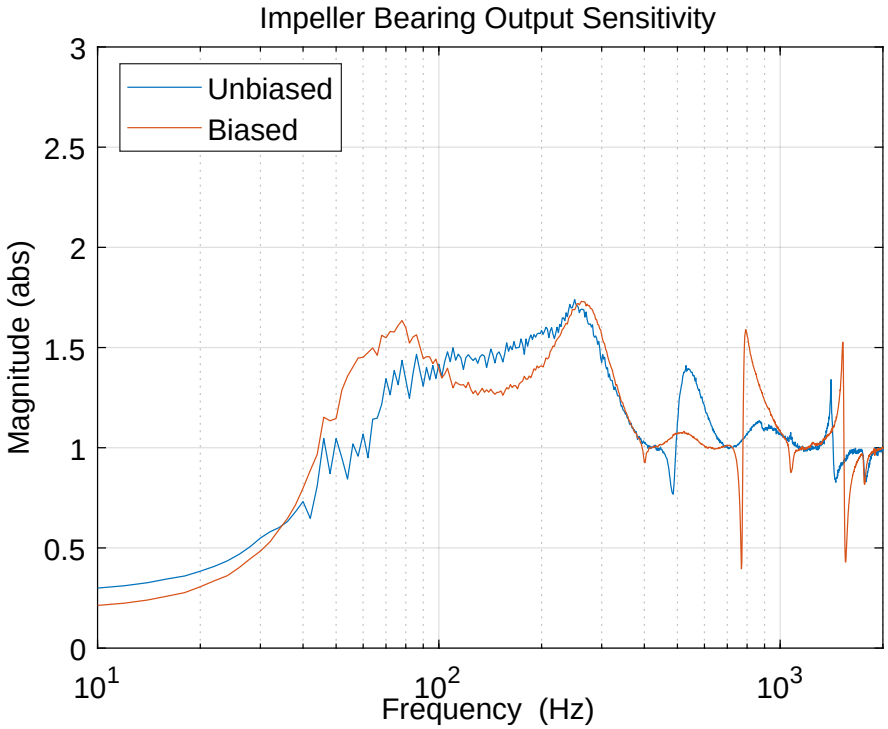

Figure 15. Comparison of output sensitivities of unbiased and biased control (impeller bearing).

Figures 16 and 17 show the vibrations at the bearing locations while spinning the rotor up to 10,000 rpm. In both cases, the peak vibrations are less than 0.02 mm. ISO 14839-2 [21] states that the vibration must be less than 30% of the allowable clearances, which is 0.06 mm for the two test rigs. Therefore, the unbiased control scheme used in

this paper limits the vibration as much as the biased counterpart, and also satisfies the performance requirements.

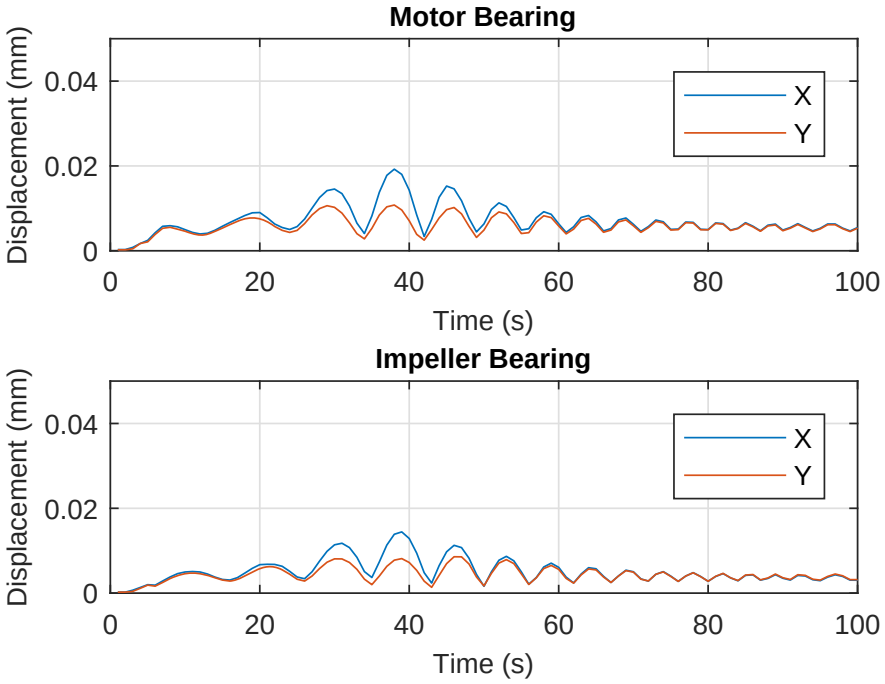

Figure 16. Displacements at the bearing locations while spinning up to 10,000 rpm (biased 8-pole system).

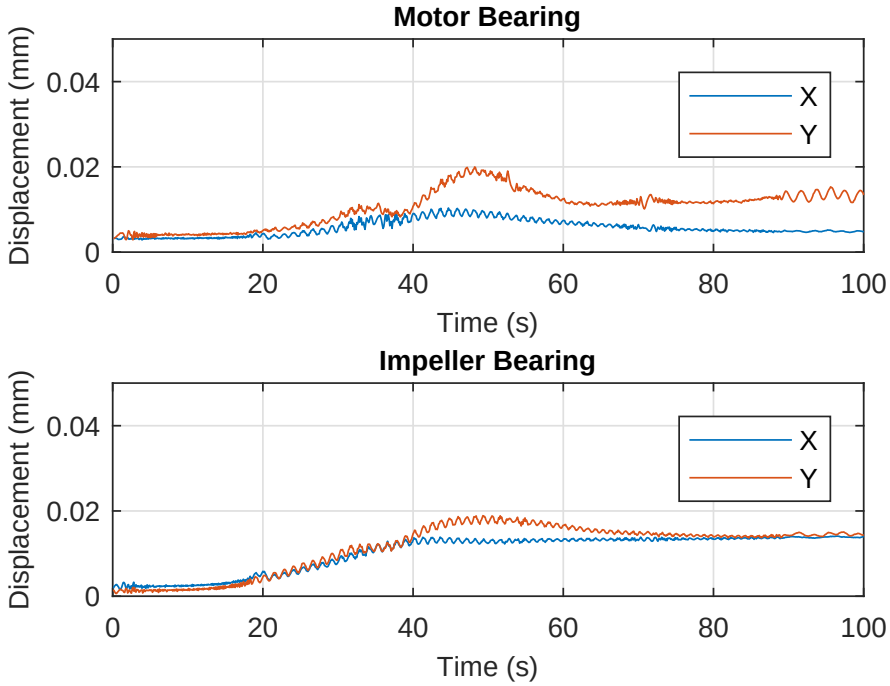

Figure 17. Displacements at the bearing locations while spinning up to 10,000 rpm (unbiased 9-pole system).

7. Conclusions

In this paper, an implementation of an unbiased control for a nine-pole radial active magnetic bearing is presented. For a fair comparison, two industry-scale compressors are built: one with conventional eight-pole symmetric bearings and another with nine-pole

unsymmetrical bearings. If the force inversion is properly performed, the plant seen by the controller is linear for the unbiased control. Therefore, a linear control algorithm can be designed and used. The experimental results confirm that the linear control algorithm for unbiased bearings satisfies both the stability and performance requirements in terms of the sensitivity and vibration levels.

The comparison of power consumption and other performance issues will be a topic of future research after developing proper metrics for comparison, such as load conditions and the variations in applied voltages.

Author Contributions: Conceptualization, methodology and writing, M.D.N.; test, data analysis, W.J. All authors have read and agreed to the published version of the manuscript.

Funding: This work was supported by the Korea Institute of Energy Technology Evaluation and Planning (KETEP) and the Ministry of Trade, Industry & Energy (MOTIE) of the Republic of Korea (Project No. 20208901010010).

Data Availability Statement: Data are contained within the article.

Conflicts of Interest: The authors declare no conflict of interest.

Appendix A. Reluctance and Coil Turn Matrix for 8-Pole Bearing

For the eight-pole symmetric radial bearing with horseshoe windings (refer to Figure 1), the reluctance matrix $\boldsymbol{\mathcal{R}}$ is defined as

$$\boldsymbol{\mathcal{R}} = \frac{1}{\mu_0}\begin{bmatrix} g_1 & -g_2 & 0 & 0 & 0 & 0 & 0 & 0 \\ 0 & g_2 & -g_3 & 0 & 0 & 0 & 0 & 0 \\ 0 & 0 & g_3 & -g_4 & 0 & 0 & 0 & 0 \\ 0 & 0 & 0 & g_4 & -g_5 & 0 & 0 & 0 \\ 0 & 0 & 0 & 0 & g_5 & -g_6 & 0 & 0 \\ 0 & 0 & 0 & 0 & 0 & g_6 & -g_7 & 0 \\ 0 & 0 & 0 & 0 & 0 & 0 & g_7 & -g_8 \\ g_0 & g_0 & g_0 & g_0 & g_0 & g_0 & g_0 & g_0 \end{bmatrix} \tag{A1}$$

The gap at each pole is a function of rotor displacements

$$g_i = g_0 - x\cos\theta_i - y\sin\theta_i,$$

where θ_i is the angle of the i-th pole.

The coil turn matrix is defined as

$$\mathbf{N} = N\begin{bmatrix} 2 & 0 & 0 & 0 \\ -1 & -1 & 0 & 0 \\ 0 & 2 & 0 & 0 \\ 0 & -1 & -1 & 0 \\ 0 & 0 & 2 & 0 \\ 0 & 0 & -1 & -1 \\ 0 & 0 & 0 & 2 \\ 0 & 0 & 0 & 0 \end{bmatrix} \tag{A2}$$

where N is the number of coil turns per pole.

Appendix B. Coil Turn Matrix for 9-Pole Bearing

For the nine-pole radial bearing with three adjacent poles wired in series (refer to Figure 2), the coil turn matrix is defined as

$$\mathbf{N} = N \begin{bmatrix} 2 & 0 & 0 \\ -2 & 0 & 0 \\ 1 & -1 & 0 \\ 0 & 2 & 0 \\ 0 & -2 & 0 \\ 0 & 1 & -1 \\ 0 & 0 & 2 \\ 0 & 0 & -2 \\ 0 & 0 & 0 \end{bmatrix} \tag{A3}$$

where N is the number of coil turns per pole.

References

1. Schweitzer, G.; Maslen, E.H. *Magnetic Bearings*; Springer: Berlin/Heidelberg, Germany, 2009.
2. Trumper, D.L.; Olson, S.M.; Subrahmanyan, P.K. Linearizing Control of Magnetic Suspension Systems. *IEEE Trans. Control Syst. Technol.* **1997**, *5*, 427–438. [CrossRef]
3. Li, L. Linearizing Magnetic Bearing Actuators by Constant Current Sum, Constant Voltage Sum, and Constant Flux Sum. *IEEE Trans. Magn.* **1999**, *35*, 528–535.
4. Charara, A.; De Miras, J.; Caron, B. Nonlinear Control of a Magnetic Levitation System without Premagnetization. *IEEE Trans. Control Syst. Technol.* **1996**, *4*, 513–523. [CrossRef]
5. Sivrioglu, S.; Nonami, K.; Saigo, M. Low Power Consumption Nonlinear Control with H∞ Compensator for a Zero-Bias Flywheel AMB System. *J. Vib. Control* **2004**, *10*, 1151–1166. [CrossRef]
6. Mystkowski, A.; Pawluszewicz, E. Nonlinear Position-Flux Zero-Bias Control for AMB System with Disturbance. *Appl. Comput. Electromagn. Soc. J. (ACES)* **2017**, *32*, 650–656.
7. De Queiroz, M.S.; Dawson, D.M. Nonlinear Control of Active Magnetic Bearings: A Backstepping Approach. *IEEE Trans. Control Syst. Technol.* **1996**, *4*, 545–552. [CrossRef]
8. Tsiotras, P.; Wilson, B.C. Zero-and Low-Bias Control Designs for Active Magnetic Bearings. *IEEE Trans. Control Syst. Technol.* **2003**, *11*, 889–904. [CrossRef]
9. Sahinkaya, M.N.; Hartavi, A.E. Variable Bias Current in Magnetic Bearings for Energy Optimization. *IEEE Trans. Magn.* **2007**, *43*, 1052–1060. [CrossRef]
10. Yoo, S.y.; Noh, M.D. An Appraisal of Power-Minimizing Control Algorithms for Active Magnetic Bearings. *Shock Vib.* **2015**, *2015*, 238629. [CrossRef]
11. Chen, S.L.; Hsu, C.T. Optimal Design of a Three-Pole Active Magnetic Bearing. *IEEE Trans. Magn.* **2002**, *38*, 3458–3466. [CrossRef]
12. Meeker, D.C.; Maslen, E.H. Analysis and Control of a Three Pole Radial Magnetic Bearing. In Proceedings of the Tenth International Symposium on Magnetic Bearings, Martigny, Switzerland, 21–23 August 2006.
13. Hemenway, N.R.; Severson, E.L. Three-Pole Magnetic Bearing Design and Actuation. *IEEE Trans. Ind. Appl.* **2020**, *56*, 6348–6359. [CrossRef]
14. Zhang, H.; Zhu, H.; Wu, M. Multi-Objective Parameter Optimization-Based Design of Six-Pole Radial Hybrid Magnetic Bearing. *IEEE J. Emerg. Sel. Top. Power Electron.* **2021**, *10*, 4526–4535. [CrossRef]
15. Meeker, D. A Generalized Unbiased Control Strategy for Radial Magnetic Bearings. *Actuators* **2017**, *6*, 1. [CrossRef]
16. Maslen, E. *Lecture Notes on Magnetic Bearings*; University of Virginia: Charlottesville, VA, USA, 2000.
17. Meeker, D.C. Optimal Solutions to the Inverse Problem in Quadratic Magnetic Actuators. Ph.D. Thesis, University of Virginia, Charlottesville, VA, USA, 1996.
18. *API617*; Axial and Centrifugal Compressors and Expanders-Compressors for Petroleum, Chemical and Gas Industry Services, American Petroleum Institute: Washington, DC, USA, 2014.
19. Messner, W.C.; Bedillion, M.D.; Xia, L.; Karns, D.C. Lead and Lag Compensators with Complex Poles and Zeros Design Formulas for Modeling and Loop Shaping. *IEEE Control Syst. Mag.* **2007**, *27*, 44–54.

20. *ISO14839-3*; Mechanical Vibration—Vibration of Rotating Machinery Equipped with Active Magnetic Bearings—Part 3: Evaluation of Stability Margin. International Organization for Standardization: Geneva, Switzerland, 2006.
21. *ISO14839-2*; Mechanical Vibration—Vibration of Rotating Machinery Equipped with Active Magnetic Bearings—Part 2: Evaluation of Vibration. International Organization for Standardization: Geneva, Switzerland, 2006.